GeoHealth

RESEARCH ARTICLE
10.1029/2018GH000175

Special Section:
Mining and Planetary Health

Measurement of OH* Generation by Pulverized Minerals Using Electron Spin Resonance Spectroscopy and Implications for the Reactivity of Planetary Regolith

Donald A. Hendrix[1], Sara T. Port[1,2], Joel A. Hurowitz[1], and Martin A. Schoonen[1,3]

[1]Department of Geosciences, State University of New York at Stony Brook, Stony Brook, NY, USA, [2]Arkansas Center for Space and Planetary Sciences, University of Arkansas, Fayetteville, AR, USA, [3]Environment, Biology, Nuclear Science & Nonproliferation, Brookhaven National Laboratory, Upton, NY, USA

Abstract Mineral analogs to silicate phases common to planetary regolith, including olivine; the pyroxenes augite and diopside; the plagioclase feldspars labradorite, bytownite, and albite; the Johnson Space Center-1A lunar regolith simulant; as well as quartz (used as a reference), were subjected to mechanical pulverization by laboratory milling for times ranging from 5 to 45 min. Pulverized minerals were then incubated in an aqueous solution containing the free radical spin trapping compound 5,5-Dimethyl-1-Pyrroline-N-Oxide for times ranging from 5 to 30 min. These slurries were then analyzed by Electron Paramagnetic Resonance spectroscopy to quantify the amount of hydroxyl radical (the neutral charge form of the hydroxide ion, denoted as OH*) formed in solution. We find that all tested materials generate an Electron Paramagnetic Resonance spectrum indicating the formation of OH* with concentrations ranging between 0.1 and 1.5 μM. We also find that, in general, mineral pulverization time is inversely correlated to OH* generation, while OH* generation is positively correlated to mineral fluid incubation time for phases that have iron in their nominal chemical formulae, suggesting the possible action of Fenton reaction as a cofactor in increasing the reactivity of these phases. Our results add to a body of literature that indicates that the finely comminuted minerals and rocks present in planetary regolith are capable of generating highly reactive and highly oxidizing radical species in solution. The results provide the foundation for further in vitro and in vivo toxicological studies to evaluate the possible health risks that future explorers visiting the surfaces of planetary bodies may face from these reactive regolith materials.

Plain Language Summary Future missions to the Moon will face many challenges and obstacles. Exposure to lunar dust will pose health risks to humans due to the reactive nature of the dust. We have assessed the reactivity of various mineral phases analogous to those present in lunar dust. Iron-rich mineral phases generate higher concentrations of hydroxyl radical relative to mineral phases with low amounts of iron. Humans working in the lunar mare may experience relatively more detrimental health effects related to regolith dust inhalation relative to those working in the lunar highlands.

Key Points:
- Electron paramagnetic resonance spectroscopy measurements show minerals with high iron content generate 2-5 times more OH* relative to minerals with low iron content
- Planetary regolith on airless bodies containing iron-rich mineral phases has the potential to generate oxidizing species that may pose a hazard to future human explorers
- High reactivity levels of iron-rich minerals should motivate the development of effective mitigation systems for humans traveling to the Moon, especially in the mare regions

Supporting Information:
- Supporting Information S1

Correspondence to:
D. A. Hendrix,
donald.hendrix@stonybrook.edu

Citation:
Hendrix, D. A., Port, S. T., Hurowitz, J. A., & Schoonen, M. A. (2019). Measurement of OH* generation by pulverized minerals using electron spin resonance spectroscopy and implications for the reactivity of planetary regolith. *GeoHealth*, *3*, 28–42. https://doi.org/10.1029/2018GH000175

Received 5 OCT 2018
Accepted 17 DEC 2018
Accepted article online 20 DEC 2018
Published online 23 JAN 2019

This article was corrected on 15 JUL 2019. The online version of this article has been modified to include a Conflict of Interest statement.

1. Introduction

Recent research has demonstrated that when silicate minerals common to Fe- and Mg-rich (mafic) igneous rocks, such as olivine, pyroxene, and plagioclase feldspar, are mechanicallypulverized in the laboratory and then mixed with liquid media, a wide variety of oxidizing compounds are generated (Cohn, Laffers, & Schoonen, 2006; Fubini et al., 2001; Hardy & Aust, 1995; Horwell et al., 2003; Hurowitz et al., 2007; Kaur et al., 2016; Loftus et al., 2010; Schoonen et al., 2006; Turci et al., 2015; Wallace et al., 2009, 2010). Some of these are compounds of oxygen and include hydrogen peroxide (H_2O_2), superoxide radical (O_2^{*-}), and OH*. Collectively, these types of oxygen-based compounds are known as reactive oxygen species or "ROS". ROS can be generated by reactions between oxygen-containing compounds (e.g., water, O_2, and H_2O_2) and broken chemical bonds present at the surfaces of mechanically pulverized minerals (Dröge, 2002; Fenoglio et al., 2001). The generation of ROS is a common and natural occurrence on Earth and can transpire in a variety of environments. For example, interactions between molecular oxygen and redox-sensitive transition metal atoms in minerals (e.g., Fe) have been demonstrated to release ROS (Harrington et al., 2015; Schoonen et al., 2006, 2010). ROS can also be generated through photolysis of nitrous acid

(HNO_2) and are major oxidants in the Earth's atmosphere (Taraborrelli et al., 2012; Zhou et al., 2001). ROS can additionally be created enzymatically within macrophages (white blood cells) attempting to remove insoluble particles that have been inhaled and deposited into the lungs (Schoonen et al., 2006). Another mechanism of ROS generation, and the focus of this work, is through interactions between water and structural defect sites at mineral surfaces. These structural defects such as E-centers and Si-O radicals are easily generated by the breaking of chemical bonds via physical processes, such as grinding, crushing, and pulverizing (e.g., Hasegawa et al., 1995). Industrial operations, such as sandblasting, and natural phenomena, such as dust storms and volcanic eruptions, are capable of generating particles with these reactive surface sites, and Fe-rich particles, which can participate in Fenton chemistry (Damby et al., 2016; Doganay et al., 2010; Haber & Weiss, 1934; Horwell et al., 2003, 2007, 2013), can stimulate further ROS generation. Equation (1) shows the Fenton reaction.

$$Fe^{2+} + H_2O_2 \rightarrow Fe^{3+} + OH^* + OH^- \quad (1)$$

On the surfaces of rocky planets, planetesimals, and asteroids, meteorite impact processes are also capable of generating fine-grained minerals with reactive surface sites that can generate ROS (Colwell et al., 2007). The thick blankets of regolith present on the surfaces of all rocky solar system bodies testify to the efficacy of this process. This dust easily adheres to surfaces; astronauts who spent time on the lunar surface during the Apollo program were quickly covered with fine-grained dust (Latch et al., 2008). Dust that adhered to their space suits was eventually brought into the Apollo spacecraft, and some astronauts exhibited allergy-like symptoms to it when inhaled (Khan-Mayberry, 2008; Scheuring et al., 2008; Wagner, 2004).

Pulverized minerals, and the ROS generated by them, are well known to be hazardous in occupational settings where dust is produced. A common exposure route is through the inhalation of fine-grained, respirable mineral dusts that generate ROS in contact with lung fluids. This exposure can result in oxidative damage and the development of lung inflammation, cardiovascular diseases, and pulmonary diseases such as silicosis over the course of long-term exposure (Caston et al., 2018; Harrington et al., 2013; King et al., 1945; Rimal et al., 2005; Vallyathan et al., 1997). ROS can also induce cell death via necrosis, which ruptures the cell membrane, or apoptosis, the programed death of a cell (Harrington et al., 2015; Schoonen et al., 2006). ROS are also known to initiate inflammation and indirectly trigger mutations and possibly cancer (Hardy & Aust, 1995; Harrington et al., 2012; Schoonen et al., 2006). High levels of iron in the body can contribute to complex reactions that lead to inflammation, fibrosis, and eventually cancer (Selby & Friedman, 1988; Stevens et al., 1986), so lunar dust, which contains abundant iron, has the potential to be a carcinogenic substance. Proposed mechanisms for ROS biotoxicity include OH* acting as an electrophile and attacking DNA molecules, which act as the nucleophiles: a process that occurs when OH* is generated in close proximity (~10 Å) to the target molecule (Pryor, 1988). Gas chromatography-mass spectrometry analysis of the byproducts of iron-catalyzed DNA damage shows that 17 different products form as a result from OH* damage of DNA (Dizdaroglu et al., 1991; Von Sonntag et al., 1991). The main product that was observed by Dizdaroglu et al. (1991) was 8-hydroxy-2′-deoxyguanosine (8-OHdG), which is a result of the oxidation of deoxyguanosine (Dizdaroglu et al., 1991). The OH* has also been linked to onset of bronchogenic carcinoma (Pezerat, 1991). These hazardous properties make ROS generation an important phenomenon to study in an effort to assess the potential health impacts to human explorers sent to planetary bodies within our solar system where fine-grained and mechanically pulverized mineral dusts formed from mafic rocks are found in abundance. This will be especially important as we move further into this century, and the possibility of space travel to planetary bodies by national space agencies or commercial spaceflight entities becomes more realistic.

Of the various ROS generated by the interaction of pulverized minerals and liquid media, OH* is among the most reactive. Previous studies show that ferromagnesian minerals (e.g., amphiboles and pyroxenes) and felsic minerals (e.g., feldspars) extracted from volcanic ash exhibit high and low OH* generation, respectively (Horwell et al., 2003). It has been shown that lunar regolith collected by the Apollo astronauts is highly reactive and that Fe content and regolith maturity are both correlated to OH* generation (McKay et al., 2015; Wallace et al., 2009). Here we present data from experiments designed to provide a quantitative measure of OH* generation from mechanically pulverized mineral phases relevant to the lunar regolith: olivine, bytownite, augite, labradorite, and diopside, as well as the lunar regolith simulant material Johnson Space Center (JSC)-1A. Owing to their extreme reactivity and short lifetimes (Pryor, 1988), we use the spin trap

compound 5,5-Dimethyl-1-Pyrroline-N-Oxide (DMPO) to sequester OH* generated by mineral powders. The signal obtained in these experiments is compared to the signal obtained in measurements of aqueous solutions with known concentrations of the stable spin standard compound 4-hydroxy-2, 2, 6, 6-tetramethylpiperidin (TEMPOL) under identical conditions. Using this strategy, OH* generation from freshly pulverized solid materials can be quantified (Eaton et al., 2010). Studies such as this provide further insights into the formation of ROS by silicate minerals and provide the framework for the mitigation of hazards that could be encountered on planetary bodies by future human explorers.

2. Methods

Our experimental protocol involved the mechanical pulverization of seven different minerals and one lunar simulant, followed by the assessment of OH* generation using an electron paramagnetic resonance (EPR)-based technique. The minerals chosen for experimentation were olivine ($(Mg,Fe)_2SiO_4$), albite ($NaAlSi_3O_8$), augite ($(Ca,Na)(Mg,Fe,Al,Ti)(Si,Al)_2O_6$), diopside ($MgCaSi_2O_6$), bytownite ($Na_{0.2}Ca_{0.8}Al_{1.8}Si_{2.2}O_8$), labradorite ($Na_{0.4}Ca_{0.6}Al_{1.6}Si_{2.4}O_8$), and quartz ($SiO_2$). Olivine, augite, bytownite, labradorite, and diopside were obtained from a mineral collection at Mount Holyoke College, curated by M.D. Dyar. Purity of these mineral phases was confirmed by X-ray diffraction and chemical compositions assessed by X-ray fluorescence (Dyar et al., 2015). Both albite and quartz were obtained as research grade mineral fragments from Wards Scientific, Inc. These seven minerals were selected due to their widespread occurrence on basaltic surfaces of planetary bodies within the solar system and because they provide a useful comparison point to the suite of minerals examined in Hurowitz et al. (2007), who analyzed the generation of H_2O_2 from these same minerals in water-mineral slurries. Quartz is not commonly found on extraterrestrial basaltic surfaces, but we used it in our experiments because it provides a reference material that is understood to be reactive and toxic (e.g., James et al., 2013; Santana et al., 2010). We also performed experiments on the lunar regolith simulant JSC-1A, which we obtained from Orbital Technologies Corporation. JSC-1A is a mass-produced version of the JSC-1 simulant, which was created by Johnson Space Center based on the composition, mineralogy, particle size, cohesion, and friction of the lunar regolith (Alshibli & Hasan, 2009). JSC-1A is meant to simulate glass-rich, low-titanium mare regolith found on the Moon. It contains crystalline silicate phases of plagioclase, pyroxene, olivine, minor oxide phases of ilmenite and chromite, and traces of clay minerals (Alshibli & Hasan, 2009). JSC-1A is not a perfect proxy of pristine lunar mare regolith, as it contains ferric iron, lower total iron abundance, traces of clay minerals, and high levels of Ti-magnetite relative to lunar regolith (Hill et al., 2007). However, reactivity data obtained from JSC-1A have value in that it is readily available to other researchers in large quantity (unlike real lunar regolith) and thus provides a reference material against which interlaboratory comparisons of reactivity can be made (Caston et al., 2018; Loftus et al., 2010; Turci et al., 2015).

Prior to grinding in a Retsch PM100 planetary ball mill, minerals were lightly crushed in a hardened-steel mortar and pestle from their as-received size of a few millimeter diameter, followed by sieving to <125 μm using a brass sieve. This crushing and sieving was not necessary for the JSC-1A sample, which is produced by Orbital Technologies Corporation as a powder. Sieved materials were then placed in a 50-ml agate grinding container fitted with three 20-mm diameter agate grinding balls and ground for 5, 15, 30, or 45 min at 350 rpm. Contamination was not a concern when using the agate ball mill because agate is well understood to produce minimal contamination when used as a grinding medium (Hickson & Juras, 1986). An aliquot of all the sample powders produced by milling in the Retch ball mill was reserved for analysis of surface area by gas adsorption (BET N_2 technique using a Quantachrome Instruments Nova 2200e Surface Area Analyzer). Based on seven measurements of a 10-m^2/g BET standard powder, we estimate uncertainties on our surface area measurements to be 6% relative at the 2-sigma level (average = 10.2 ± 0.6, 2σ).

Scanning electron microscopy (SEM) was used to image pulverized mineral samples using a LEO-1550 FEG SEM equipped with an energy dispersive X-ray (EDAX) spectrometer, which was used to obtain energy-dispersive X-ray spectra from our pulverized mineral samples in order to obtain qualitative information on their chemical compositions. All samples were coated twice with a 2-nm gold layer using an Edwards 150B sputter coater at a 30° angle prior to SEM/EDAX analysis. SEM images and EDAX spectra are presented in the supporting information (Figures S1–S28). Grain size distribution data were obtained for a

subset of samples that were ground for 5, 15, and 30 min using a Malvern Instruments Mastersizer 2000, which measures the light scattering intensity of particles suspended in deionized water to determine particle sizes. Grain size distribution curves are shown in the supporting information (Figures S29–S35). Grain size information of JSC-1A is available from Zeng et al. (2010).

After completion of each individual grinding cycle, the samples were separated into individual Al-foil wrapped, 15-ml centrifuge tubes and incubated in solution for 5, 15, 30, or 45 min. Each vial contained 0.5 ml of 40-mM DMPO to which 200 mg of ground sample was added. For the duration of the incubation, the sample-DMPO slurry was placed on an end-over-end tube rotator to mix the DMPO and mineral powder, promote reaction between DMPO and OH*, and generate the stable DMPO-OH adduct. Following incubation, each slurry was filtered using either a 0.02- or a 0.1-μm syringe filter. Then, 50 μl of the filtered solution was pipetted into a capillary EPR tube and inserted into the sample cavity of a Magnettech MS400 MiniScope EPR spectrometer to determine the OH* concentration generated in solution by the pulverized solid sample. The EPR measurements were typically carried out within ~5 min of completing the incubation; early experiments with DMPO revealed that the DMPO-OH adduct has a limited lifetime. Based on our experience, we estimate that waiting longer than ~10–20 min to make the EPR measurement of DMPO-OH has a noticeable effect on the final determination of OH* concentration. This finding is in general agreement with experimental data on the half-life of DMPO-OH, determined to be 16.6 min for a 50-μM DMPO-OH solution (Nakamura et al., 2010).

To measure OH* generation, we adapted an experimental protocol that makes use of the radical spin trapping compound DMPO to measure OH* generation from pulverized minerals (Eaton et al., 2010; Horwell et al., 2003; Turci et al., 2015). DMPO stabilizes the OH* generated by pulverized minerals as a DMPO-OH radical adduct. This stable adduct, or "spin trap," is then measured by EPR spectroscopy. In order to quantify OH* generation, we used the spin standard TEMPOL at concentrations of 0.5, 1.0, 2.0, and 3.0 μM. These solutions were measured on the EPR spectrometer using identical scan parameters to those used for measurement of experimental DMPO solutions. A set of EPR spectra collected on TEMPOL solutions with concentrations ranging from 0.5 to 3 μM are shown in the supporting information (Figure S36).

The MS400 spectrometer is an X-band EPR spectrometer, operating at microwave frequencies between 9.3 and 9.55 GHz. For measurement of EPR spectra, we typically used a magnetic field center point (B_o) of 3,360 gauss (G) and swept the instrument through a magnetic field range of approximately 80 G, using a 60-s sweep time. Other instrument settings included a modulation amplitude of 3,000 mG and a microwave power of 32–50 mW (equivalent to a microwave attenuation of 3–5 dB). Finally, we note that, because EPR spectroscopy makes use of a phase-sensitive detection scheme, the microwave absorbance spectra are recorded as first-derivative spectra and plotted as graphs of $\frac{dA}{dG}$ versus G, where A is microwave absorbance and G is magnetic field strength in units of Gauss. Accordingly, quantification of total microwave absorbance typically involves fitting and removal of the spectral baseline, integration of the derivative spectra to convert it into an absorbance spectrum, followed by a second integration to calculate the area under the absorbance curve.

An alternative approach used here is simply to measure "β" (Figure S37), the absolute value of the height of one of the characteristic peaks in the first-derivative spectra of the compound being measured (Rice-Evans et al., 1991). We made use of this approach because we found that our EPR measurements, particularly at low-spin trap concentration, were characterized by an irregularly sloping baseline that could not be readily subtracted from our EPR spectra. All attempts to perform a double integration of the first-derivative EPR spectra after baseline subtraction produced abnormal integral curve shapes. Accordingly, we have adopted the more straightforward measurement of β for our purposes. We find a linear scaling relationship between our measurements of β and the known concentration of the TEMPOL solution in our measurement range (Figure S38). Standard curves were constructed at the beginning of each measurement session and used for determination of the concentration of OH* generated in mineral-DMPO experimental slurries. This determination was made by measurement of the β value for the second, larger peak in each spectrum collected on DMPO-OH experimental solutions (Figure S39), followed by comparison of the measured β value to the calibration curve of β versus TEMPOL concentration.

In addition to the incubations described above, we assessed the reactivities of quartz and augite as a function of time in order to understand how long minerals can be expected to retain their reactive properties in a lab

air environment after they have been mechanically pulverized. These minerals were chosen due to their wide variations in reactivity (described below). For these experiments, powdered samples were left out on the benchtop after pulverization and reactivity measurements were performed on additional aliquots of those samples every 1–2 days without further grinding. Approximately 15 g of augite and quartz were ground in an agate ball mill grinder for 15 min before testing. For each experiment, approximately 200 mg of sample was incubated for 15 min in 88.4-mM DMPO before DMPO-OH concentration determinations with EPR.

In order to determine whether iron was being released into solution during incubation of our mineral slurries (labradorite, bytownite, augite, forsterite, albite, quartz, and diopside), we measured dissolved iron concentrations using a Thermo iCAP 6300 radial view inductively coupled plasma-atomic emission spectrometer (ICP-AES). Each sample was incubated for 30 min using the same procedure as those used to prepare samples for EPR analysis. The filtrates were then placed into a 20-ml plastic vial which was then added 1.5-ml 5.0% HNO_3 solution. The concentrations of iron in the unknowns were determined using 0.1, 1.0, and 10.0 ppm Fe standard solutions. The intent of these measurements was to assess whether dissolved Fe, derived from the minerals during incubation, was playing a role in the generation of OH* via Fenton's reaction (equation (1)).

Finally, because DMPO-OH spectra can also be produced by interaction between DMPO and Fe^{3+} (Cohn, Mueller, Wimmer, et al., 2006; Makino et al., 1990), we performed a control experiment to demonstrate that our DMPO-OH spectra were produced as a result of interaction between DMPO and OH*, rather than DMPO and Fe^{3+}. In these control experiments, we combined 20 μl of high-purity methanol, 50 μl of a 2.5-mM $FeCl_2{\cdot}4H_2O$ solution, 20 μl of a 4.45-mM H_2O_2 solution, and 1 ml of a 88.4-mM DMPO solution then incubated them for 5 min in a 15-ml centrifuge tube on an end-over-end rotisserie. The mixture of Fe^{2+} and H_2O_2 results in the formation of OH* by the Fenton reaction. The methanol effectively competes with DMPO to scavenge the OH*, and the resulting methanol-based radical goes on to react with DMPO. The resulting EPR spectrum, which results from the interaction between DMPO and a methanol-based radical that was formed by interaction with OH*, provides indirect confirmation that OH* was present in solution. This spectrum can then be used as the basis for comparison to a spectrum generated by adding 20 μl of methanol to an olivine-DMPO slurry, which was incubated under the same conditions and measured by EPR.

3. Results

3.1. Measurement Accuracy and Repeatability

One of the challenges faced in developing a protocol to quantify OH* generation on the basis of EPR spectroscopy using spin trapping is to evaluate the uncertainty in the measurements. We attempt to provide an assessment of the accuracy associated with the OH* concentrations using our TEMPOL calibration curves, as follows. For each TEMPOL calibration curve constructed, we performed four linear regressions on the data set, each time leaving one of the four data points (0.5, 1.0, 2.0, and 3.0 μM) out of the regression. We then used the equation for the linear regression through the remaining three data points to calculate the TEMPOL concentration of the data point that was left out of the regression, effectively treating that measurement of a standard as an unknown. We then estimated the accuracy of our measurements by calculation of percent error, defined here as

$$\left[\frac{(|\text{Calculated TEMPOL Concentration}-\text{Known TEMPOL Concentration}|)}{\text{Known TEMPOL Concentration}}\right]*100$$

and found that at 0.5, 1.0, 2.0, and 3.0 μM, accuracy, expressed as percent error, came out to 0–60%, 0.93–7%, 0.76–4%, and 2.88–6%, for the full set of TEMPOL calibration curves constructed during the course of our experimental measurements, respectively.

The repeatability (i.e., precision) of our experimental protocol was evaluated on the basis of 30 duplicate measurements (9 duplicates for olivine, 9 duplicates for albite, and 12 duplicates for JSC-1A), shown in Table 1. Because each of our replicate measurements represents a distinct set of grind and incubation times, as well as differing solid substrates (i.e., olivine, albite, and JSC-1A), it is not possible for us to determine a statistically meaningful aggregate value for measurement precision. We do note that Kaur et al. (2016) estimated the precision of the same protocol as ours, on the basis of triplicate measurement with JSC-1A

Table 1
Surface Area-Normalized OH Concentration Values (μmol/m²)*

Grind time (min)	Incubation time (min)	Olivine		Albite		Bytownite		JSC-1A		Augite		Diopside		Quartz		Labradorite	
5	5	1.40	4.40	1.03	2.39	1.15	0.77	1.60	—	—	7.87	—	1.96	—	1.24	—	0.31
	15	3.60	5.28	0.91	3.30	1.25	1.18	2.11	—	—	7.41	—	2.15	—	1.05	—	0.36
	30	4.59	6.01	1.24	2.57	—	0.89	2.18	—	—	8.33	—	2.88	—	1.37	—	0.49
15	5	5.20	6.16	0.68	1.38	1.14	1.53	2.21	—	—	3.47	—	1.80	—	0.74	—	1.04
	15	6.76	7.53	0.68	1.34	1.06	1.22	2.66	—	—	4.44	—	2.53	—	0.74	—	0.82
	30	7.50	7.46	0.86	1.56	0.98	1.06	2.13	—	—	5.23	—	3.69	—	0.81	—	0.67
30	5	3.29	4.91	0.45	0.97	0.67	0.93	2.25	—	—	2.68	—	2.23	—	0.80	—	0.94
	15	4.68	5.99	0.42	0.97	0.85	0.90	2.43	—	—	4.15	—	2.48	—	0.74	—	0.73
	30	5.81	6.51	0.31	0.97	0.75	0.69	2.86	—	—	4.54	—	2.90	—	0.98	—	0.68
45	5	2.58	—	0.30	—	—	—	1.70	—	1.41	—	1.29	—	—	—	—	—
	15	3.97	—	0.28	—	—	—	2.21	—	2.09	—	1.29	—	—	—	—	—
	30	4.52	—	0.28	—	—	—	2.36	—	2.33	—	1.59	—	—	—	—	—

material on the same equipment used in this study, to be ±0.1 μM for a sample that yielded a mean OH* concentration of 0.6 μM (or ±16.7% relative). For our replicate data, we present an alternate approach that is often used in biomedical research to assess measurement repeatability (Bland & Altman, 1986). In this approach, the difference between individual replicates is calculated and then a mean and standard deviation of all differences are calculated. For the replicates in Table 1, this results in a mean difference of −0.23 μM with a 2σ value of ±0.70 μM for olivine, a mean difference of −0.07 μM with a 2σ value of ±0.23 μM for albite, and a mean difference of 0.07 μM with a 2σ value of ±0.41 μM for JSC-1A. If the measurements are to be considered repeatable, then the differences between individual replicate measurements must lie within two standard deviations of the mean difference of all replicates. Graphically, this is presented in a Bland-Altman plot (Figures 1a–1c), where the difference between individual replicates is plotted against the mean of the individual replicates. Here it can be seen that the differences between our individual replicate measurements lie within the calculated 2σ envelope, indicating that our measurements meet the criteria required to consider them repeatable (Bland & Altman, 1986).

3.2. OH* Generation by Pulverized Solids

Surface area-normalized OH* concentration values (μmol/m²) are presented in Table 1. Values for μmol OH* were calculated using the OH* concentrations determined in solution by EPR spectroscopy (presented in supporting information Table S1 as a function of grind time and incubation time) and the measured volume of liquid (L) used to generate a sample-DMPO slurry in each experiment. Values for square meter were determined from surface area measurements (m²/g), shown in Table 2, and the measured mass of solid sample (g) used to generate a sample-DMPO slurry in each experiment. We will generally refer to these surface area-normalized OH* generation values as the basis for discussion of our experimental results. Finally, average grain sizes measured by light scattering are presented in Table 3.

3.2.1. Olivine

As illustrated in Figure 2a, OH* generation increased with increasing incubation time for all experiments, representing four different total periods of grinding. However, OH* generation does not increase with prolonged grinding as may be expected. Prolonging grinding from 5 to 15 min does increase the generation of OH*, but any further grinding decreases OH* generation. In fact, at the longest incubation period, the OH* generation for olivine ground for 45 min is no different from olivine ground for 5 min. Surface area increases slightly with increasing grind time and grain size decreases, as might be expected. Compared to other minerals and JSC-1A tested in this study, olivine generates the highest levels of OH* under almost all experimental conditions tested (Table 1).

3.2.2. Pyroxenes

As shown in Figures 2b and 2c, augite and diopside generally exhibit increased generation of OH* with increasing incubation time. Both pyroxenes exhibit similar relationships between OH* generation and grind time. The 5-min grind time generated the most OH*, followed by the 15-, 30-, and 45 min grind times.

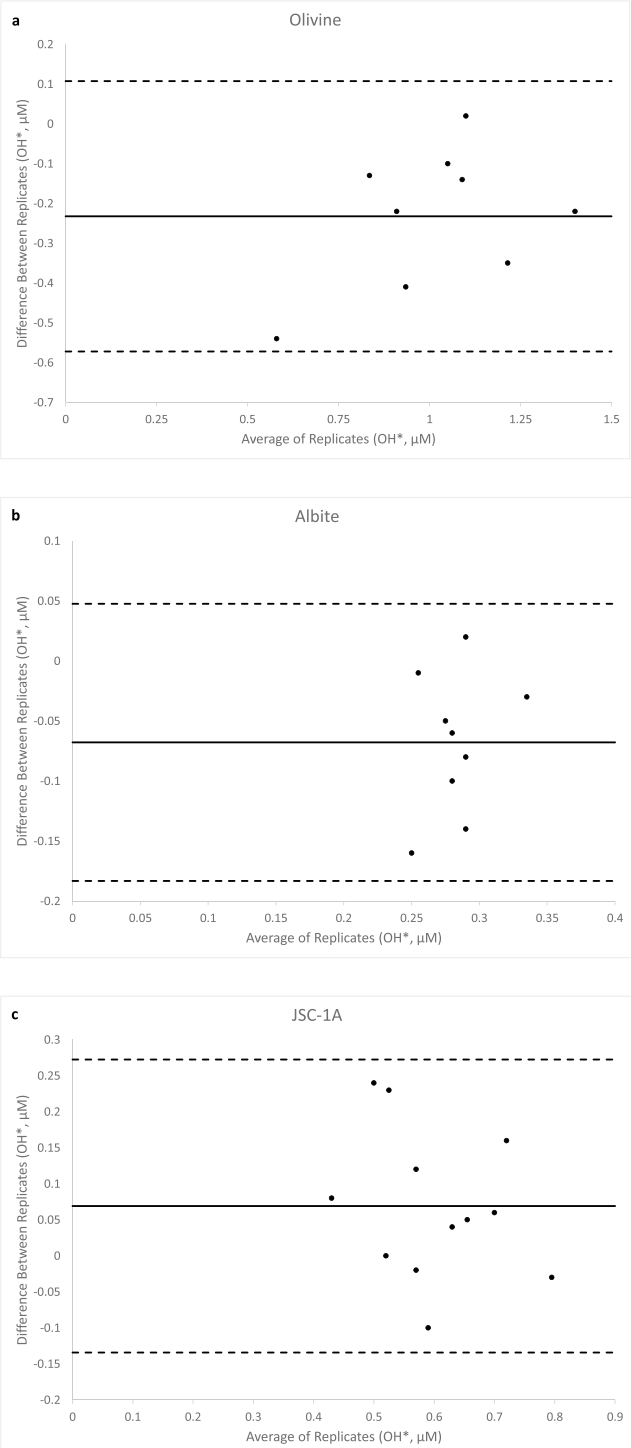

Figure 1. (a–c) Bland-Altman diagram showing the relationship between the average value of replicate measurements and the difference between replicate measurements compared to the mean difference between replicates as well as the 2σ error on the mean difference (dashed horizontal lines) for olivine, albite, and JSC-1A. Points that fall within the 2σ error envelope meet the statistical criteria to be considered repeatable measurements. JSC-1A = Johnson Space Center-1A. OH* = Hydroxide ion.

3.2.3. Lunar Simulant, JSC-1A

As illustrated in Figure 2d, OH* generation generally increases with increasing incubation time, though the 15-min grind, 30-min incubation experiment defies this general trend. OH* generation does not appear to exhibit any clear dependence on grinding time, and surface area seems to be relatively invariant as a function of grinding time for the JSC-1A simulant. JSC-1A simulant seems to generate OH* at concentrations intermediate between the individual mineral phase experiments, likely a result of the fact that JSC-1A is a mixture of mineral phases.

3.2.4. Feldspars

As illustrated in Figures 2e–2g, OH* generation shows no consistent trend with increasing incubation time in the presence of DMPO. In contrast, OH* generation shows a clear decrease with increased grind time from 5 to 45 min, regardless of incubation time, while surface area increases with increasing grind time. As illustrated in Figures 2e–2g, OH* generation from bytownite shows no consistent trend with increasing incubation time in the presence of DMPO, similar to albite. In some cases, OH* generation seems to decrease with increased grind time from 5 to 30 min; in others, reactivity rises with grind time before subsiding upon further grinding. Broadly, results for bytownite are generally in accord with those for albite. Figures 2e–2g illustrate how labradorite generates OH* similarly to both albite and bytownite. Prolonged incubation times seem to lead to decreases in the generation of OH* with the exception of the 5-min ground bytownite which exhibited a slight increase in OH* generation with increased incubation time.

3.2.5. Quartz

Quartz generated the least amount of OH* relative to all the other minerals, and no consistent trend can be ascertained regarding grind time and incubation time. Figure 2h shows the OH* generation trends of quartz.

3.3. ICP-AES

Dissolved iron was not present in our sample slurries at concentrations above the detection limit of ICP-AES, which we determined to be ~1.0 µM. This detection limit is similar to the maximum OH* values measured in our experiments (Table 1). Therefore, we are unable to unambiguously determine whether dissolved iron derived from mineral dissolution played a role in the generation of OH* in our mineral-DMPO slurries.

3.4. Reactivity Versus Time

It can be seen in Figure 3 that both augite and quartz OH* generation decrease as a function of time. Quartz generated ~0.5-µM OH* upon initial grinding, then rapidly decreased in reactivity, generating little to no measurable OH* with prolonged exposure to lab air. Augite generated higher concentrations of OH* (~0.9 µM) compared to quartz and maintained this relatively high reactivity until approximately 96 hr after initial grinding, after which point, little to no measurable OH* was generated.

3.5. SEM and EDX

SEM and EDX were used to assess how the particle shape and size change as a function of grind time and to detect any possible contamination from the grinding medium. SEM images reveal that all samples experienced size reduction and increased angularity as grinding time increased, and

Table 2
Surface Area (m^2/g) for All Solid Phases

Grind time (min)	Olivine	Albite	Bytownite	JSC-1A	Augite	Diopside	Quartz	Labradorite
5	1.11	1.21	0.96	1.47	—	—	—	—
	0.97	0.55	0.84	—	0.54	1.10	0.76	1.12
15	0.74	1.85	1.32	1.22	—	—	—	—
	0.73	1.12	0.95	—	1.20	1.17	0.68	0.67
30	1.11	2.77	2.01	1.40	—	—	—	—
	1.16	1.70	1.45	—	1.53	1.55	0.81	1.17
45	1.55	4.13	—	1.65	2.06	2.45	—	—
	—	—	—	—	—	—	—	—

Note. Em dash = not determined. JSC-1A = Johnson Space Center-1A.

there was no obvious evidence of foreign contaminants for all mineral phases as determined by SEM or EDX (supporting information Figures S1–S35).

3.6. Methanol Test for OH* Generation

As shown in Figure 4, the spectrum for the mixture of methanol, DMPO, and Fenton reagent is identical to that measured for a slurry of methanol, DMPO, and olivine powder, demonstrating that our mineral samples are generating OH* in solution and that our DMPO-OH spectra from mineral slurries do not result from interaction between DMPO and Fe^{3+}.

3.7. Correlations Between OH* Generation and FeO Content

Figure 5 shows a plot that compares the relationship between OH* generation and FeO wt.% for each mineral (Fe concentration derived from X-ray fluorescence analysis is shown in Table 4), where it can be seen that augite and olivine generated the most OH* and contain the largest amounts of bulk iron compared to any other mineral. Linear regression analysis shows an r^2 value of 0.91 indicating a strong correlation between FeO content and OH* generation capability. We note that the lunar surface is rich in iron oxides such as ilmenite, which are not included in this study. Further research involving a reactivity assessment of iron-rich oxide minerals relevant to the lunar surface would lend further insight into the potential reactivity of lunar regolith.

4. Discussion

4.1. Controls on Reactivity

Our results demonstrate that OH* generation by various silicate minerals and a lunar simulant can be reliably quantified by EPR spectroscopy when mineral slurries are prepared in the presence of the radical spin trapping compound DMPO. Quantification is achieved through the use of calibration curves based on EPR measurements of the spin standard compound TEMPOL, and integration of the first-derivative EPR spectra is not required to achieve quantitative results. Instead, measurement of β, the absolute value of the height of the first-derivative spectra, provides a reasonable approximation of total microwave absorption, which is proportional to the concentration of the EPR-active compound being measured.

Our results are in general accord with those of Hurowitz et al. (2007) who demonstrated the following order of reactivity from greatest to least, olivine > pyroxene (augite, diopside) > feldspar (labradorite), in terms of H_2O_2 generation by mineral slurries that were generated by mixing freshly ground minerals with ultrapure

Table 3
Average Grain Sizes (μm) for All Mineral Phases

Grind time (min)	Olivine	Bytownite	Albite	Augite	Diopside	Quartz	Labradorite
5	26.78	35.54	21.13	29.60	16.61	23.35	19.30
15	21.22	16.89	11.27	22.19	11.91	17.74	11.65
30	20.03	11.20	8.12	17.94	11.21	11.73	9.32

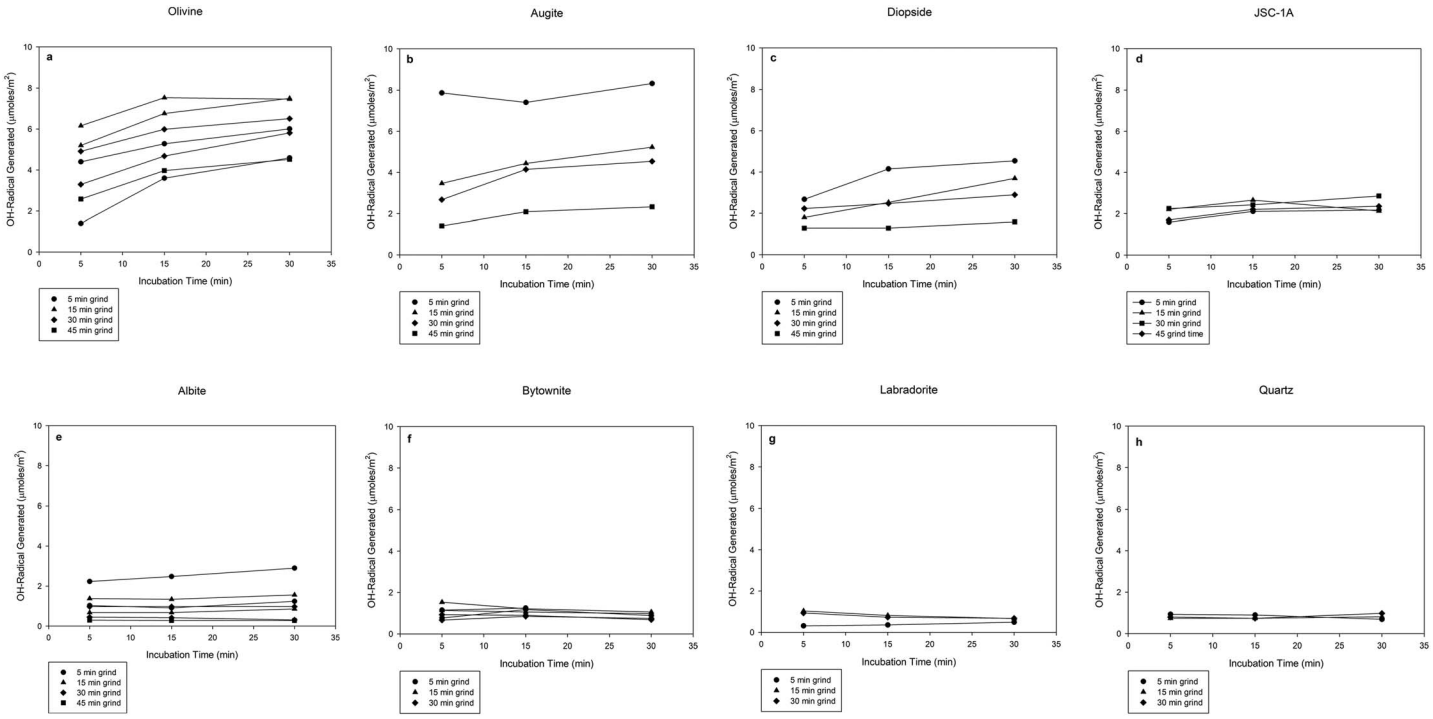

Figure 2. (a–h) OH* generation in units of micromoles per square meter versus incubation time in the presence of DMPO-OH for olivine, augite, diopside, JSC-1A, albite, bytownite, labradorite, and quartz subjected to grinding times of 5, 15, 30, and 45 min. OH* = Hydroxide ion; DMPO-OH = 5,5-Dimethyl-1-Pyrroline-N-Oxide-Hydroxide; JSC-1A = Johnson Space Center-1A.

water and measured using a fluorescence technique sensitive to H_2O_2. The details of our experimental protocols differ enough from those of Hurowitz et al. (2007) to prevent a direct quantitative comparison of H_2O_2 generation to the OH* generation measurements presented here, but the general trends for OH* generation are the same as for H_2O_2, with olivine > pyroxene (augite, diopside) > feldspar (albite, bytownite, labradorite) > quartz (Figure 6). It is perhaps unsurprising that the JSC-1A simulant, being a mixture of plagioclase, pyroxene, olivine, and other igneous mineral phases, generally generates OH* concentrations that are intermediate between the pure mineral phases used in this study.

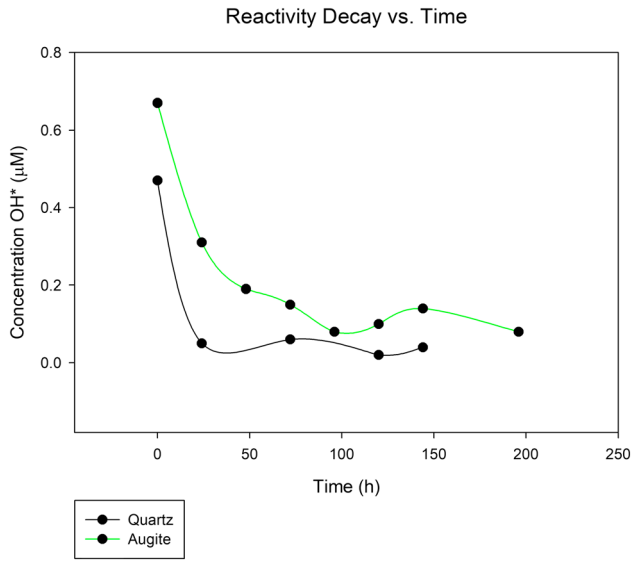

Figure 3. Reactivity (OH* generation) versus time (hours powder is exposed to atmosphere) of both augite and quartz. OH* = Hydroxide ion.

Nominally Fe-free minerals, such as quartz and albite (Table 4), are capable of generating OH*, indicating that the generation of this radical species can occur as a result of reactions between Fe-free defect sites and water, consistent with previous studies (e.g., Turci et al., 2015). However, our observation that OH* concentrations increase in the presence of Fe-bearing minerals suggests some role for Fenton chemistry. Unfortunately, our ICP-AES analysis was not able to verify whether OH* generation is a strictly surface-mediated process or is taking place in solution in the presence of dissolved iron. Other studies have alluded to the fact that Fenton chemistry can result from surface-mediated processes involving defect sites that contain Fe^{2+} (Horwell et al., 2003; Turci et al., 2015). Using techniques with more sensitive detection limits such as inductively coupled plasma-mass spectrometry may give a more definite answer as to whether this is a strictly surface-mediated process or a mix between solution and surface-mediated process. Regardless, reaction between H_2O_2 and surface-Fe sites or dissolved Fe will yield the same result via Fenton chemistry: the generation of OH*. In the case of our

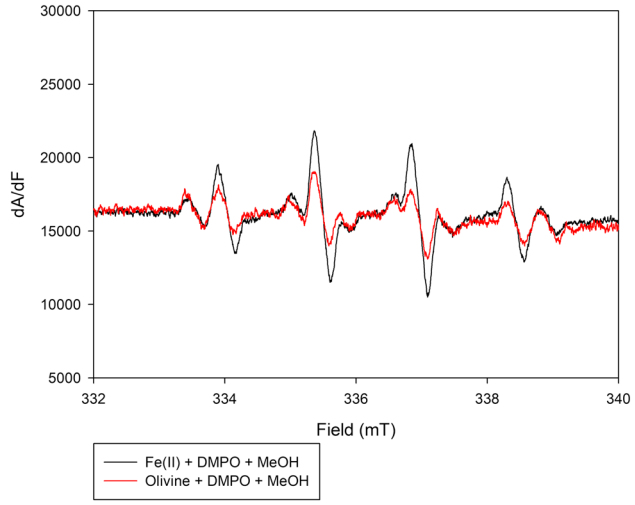

Figure 4. The similarities in peak structure between the red and black spectra indicate that methanol is scavenging OH* generated in solution by both Fe (II) solution and olivine. OH* = Hydroxide ion; DMPO = 5,5-Dimethyl-1-Pyrroline-N-Oxide.

slurry experiments, a ready source of H_2O_2 is provided by reactions between pulverized mineral surfaces and H_2O, as demonstrated by, for example, Hurowitz et al. (2007).

One of the more surprising results of our study is that, in general, we observe that increased grinding time is inversely correlated to surface area normalized OH* generation. A reasonable a priori assumption is that increased grinding time should result in the production of increasingly finer particulates, higher surface area, and a larger concentration of broken surface bonds available to generate ROS when immersed in solution. Instead, we found that increased grind time did not always result in dramatically increased surface area, indicating that we may have approached a limit to continued size reduction with increased grinding time. We noticed during experimentation that the grinding container grew warmer with increased grinding time and suggest that the frictional heating that occurred as a result of mechanical interaction among the grinding container, grinding balls, and the mineral particulates in the container may have acted to anneal reactive surface sites that were generated in the early stages of the grinding activity.

Our results regarding the effect of incubation time on total OH* generation seems to indicate that incubation time generally has either no effect (albite, bytownite, diopside, labradorite, and quartz) or a positive effect (olivine, augite, and JSC-1A) on total OH* generation. Within these results, it is difficult to disentangle the competing effects of OH* generation by the mineral and decay of the DMPO-OH adduct, which has a half-life of ~15 min (Nakamura et al., 2010). We suggest that, for those experiments in which OH* concentrations were not strongly influenced by incubation time, a quasi steady state condition between OH* generation and DMPO-OH decay was achieved during the incubation. For experiments in which OH* concentrations increased with incubation time, (olivine in particular), the results likely indicate that the mineral had enough reactive surface sites to generate OH* at a rate that exceeded the rate of DMPO-OH decay. An additional factor, which may have added to the more rapid generation of OH* in some cases, is through interaction between Fe^{2+} (at the mineral surface or released by dissolution) and H_2O_2 generated by reactions between water and defect sites at the mineral surface. Mechanical alteration of mineral surfaces increases the amount of silica radicals on the surface (Fubini et al., 2001; Hasegawa et al., 1995). Silica radicals could then react with water to generate hydrogen peroxide which then could react with any surface iron via the Fenton reaction to generate OH* as shown in reactions (2) and (3).

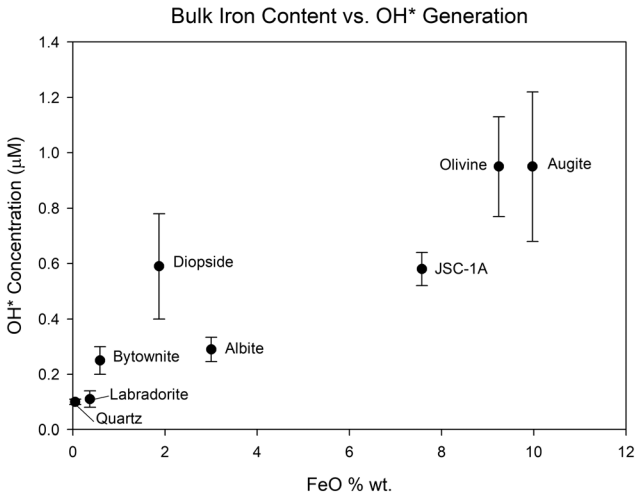

Figure 5. FeO% wt. versus OH* generation of albite, quartz, bytownite, labradorite, augite, diopside, JSC-1A, and olivine. Data are the average of all the 5-, 15-, and 30-min incubation times for the 15-min ground samples (linear regression through the data yields an $r^2 = 0.91$). OH* = Hydroxide ion; JSC-1A = Johnson Space Center-1A.

$$2\ \equiv Si{-}O\cdot + 2\ H_2O \rightarrow 2\ \equiv Si{-}OH + H_2O_2 \quad (2)$$

$$\equiv Fe^{2+} + H_2O_2 \rightarrow \equiv Fe^{3+} + \cdot OH + {}^{-}OH \quad (3)$$

While more studies are needed, it is possible that reaction (2) may be responsible for the hydrogen peroxide measured by Hurowitz et al. (2007). Kaur et al. (2016) measured hydrogen peroxide generation from lunar simulants, including JSC-1A in DI water, and found that hydrogen peroxide was generated in experiments conducted in air and in a N_2-purged glove bag; both conditions generated H_2O_2 at similar levels (Kaur et al., 2016). It is interesting to note that the materials that contain Fe as a component of their nominal chemical formulae exhibit a relationship between incubation time and OH* generation (olivine, augite, and JSC-1A), whereas those without iron in their nominal chemical formulae generally exhibit no distinguishable trend with incubation time (albite, bytownite, diopside, and labradorite). These results are consistent with previous work using a range of ROS-sensitive measurement techniques

Table 4
Solid Phase Composition Data Determined by XRF[a]

Component	Olivine	Diopside	Augite	JSC-1A[b]	Labradorite	Bytownite	Albite[c]	Quartz[c]
SiO_2	41.10	53.89	53.35	46.67	52.74	51.68	73.7	99.3
Al_2O_3	0.01	0.01	0.51	15.79	29.86	30.24	18.9	0.59
TiO_2	0.01	0.01	0.01	1.71	0.07	0.05	0.05	0.06
FeO	9.24	1.87	9.97	7.57	0.37	0.59	0.03	0.05
MgO	50.38	16.54	12.08	9.39	0.11	0.14	—	—
MnO	0.14	0.07	0.28	0.19	—	—	—	—
NiO	0.34	0.04	0.02	—	—	—	—	—
Cr_2O_3	0.03	0.01	0.03	—	—	—	—	—
CaO	0.08	24.74	23.25	9.90	12.21	13.29	0.29	0.04
Na_2O	0.01	0.39	0.46	2.83	4.47	3.79	6.77	—
K_2O	—	—	—	0.78	0.26	0.21	0.19	—

Note. Em dash = not determined. XRF = X-ray fluorescence; JSC-1A = Johnson Space Center-1A.
[a]All values in percent weight. [b]Data from Orbital Technologies Corporation (ORBITEC). [c]Semiquantitative compositional data for quartz and albite were determined by energy dispersive X-ray spectroscopy at Stony Brook University.

and suggest a possible important role for Fenton chemistry as a cofactor in the generation of OH* in our experiments (Schoonen et al., 2006).

Finally, the reactivity of an Fe-free (quartz) and Fe-bearing (augite) mineral was compared as a function of time, as seen in Figure 3, where it can be seen that quartz reactivity dissipates much more rapidly compared to augite. This may be due to the large availability of iron in augite relative to quartz. Wallace et al. (2009) showed that freshly pulverized quartz approached the reactivity of unground quartz in approximately 10 hr, while JSC-1A took about 24 hr to reach such a level. Wallace et al. (2009) conducted experiments comparing the reactivity decay through time between JSC-1A and quartz. They left both of these samples in sample chambers that were approximately 25 °C and at around 50% humidity after the samples were ground by hand using a mortar and pestle. The samples were not ground upon further reactivity experiments. They measured the amount of OH* using a terephthalate assay which involves the fluorescence measurements of the product formed due to oxidation of terephthalate via OH*. Overall, our results are in agreement with Wallace et al. (2009). Accordingly, we suggest that any dust lingering inside a lunar habitat would likely see its reactivity diminish through time.

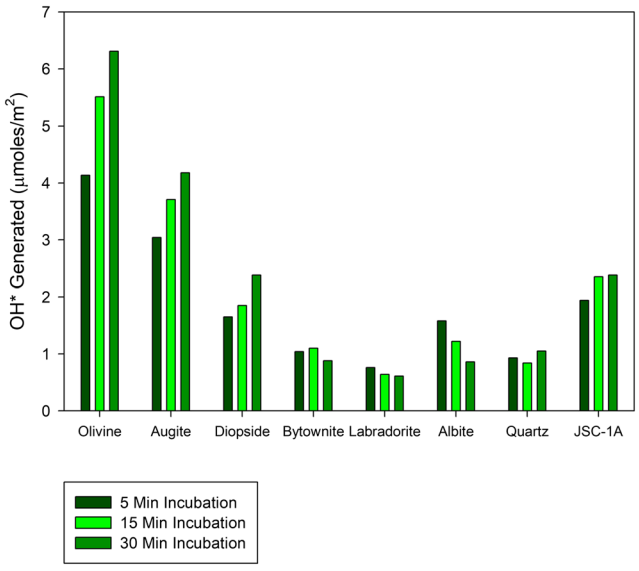

Figure 6. Average OH* generation in units of micromoles per square meter for all grind experiments. Data shown for 5-, 15-, and 30-min incubations in the presence of DMPO-OH. OH* = Hydroxide ion; JSC-1A = Johnson Space Center-1A.

4.2. Potential Implications for Astronaut Health

Particles smaller than 10 μm accumulate in the lungs and cause diseases such as bronchitis and asthma, and any particle smaller than 4 μm would accumulate in the alveolus and could eventually lead to silicosis and cancer (Beckett, 2000). Particles that are able to be uptaken by the human respiratory system will be of great concern for future lunar explorers. Locations where particles can travel within the respiratory system is shown as a function of grain size in Figure 7 (Horwell et al., 2007).

While our work does not focus on nanosized particles, it is important to note that nanosized particles would have the potential to be absorbed by the lymphatic system or nervous system which would then enable the dispersion of lunar dust and np-Fe throughout the body (Dodson et al., 2007; Orberdörster et al., 2005). Particle size distributions (PSD), which are plots of grain size versus quantitative abundance, of Apollo 14 soil show that there are particles in lunar dust as small as a few tens of nanometers in diameter, which highlights the potential health risks of being exposed to lunar dust (McKay et al., 2015). Our work adds to a growing body of literature that has established that finely pulverized mineral and rock fragments present in the regolith of planetary surfaces in our solar system have the potential to spontaneously generate ROS when exposed to humid

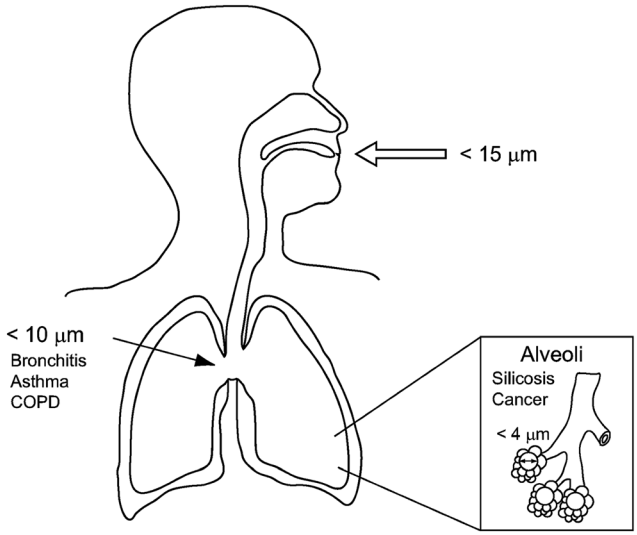

Figure 7. Diagram showing the areas where particulate matter is able to settle inside the human respiratory system as a function of particle size. Figure from Horwell et al. (2007)—Reproduced by permission of The Royal Society of Chemistry. COPD = chronic obstructive pulmonary disease.

environments such as the human respiratory system. Dust migrated inside a human habitat from the vacuum environment of space is predicted to exhibit elevated reactivity levels relative to Earth dusts. The OH* generation demonstrated to occur here is of particular interest given the reactivity of this ROS species toward organic compounds, biomolecules, and genetic material, such as DNA and RNA (Caston et al., 2018; Fubini & Hubbard, 2003; Gilmour et al., 1995; Linnarsson at al. 2012; Schoonen et al., 2006). These results suggest that inhalation exposure may lead to bodily harm.

Previous studies have shown that quartz dust generates greater toxicity responses in rats compared to lunar dust (sample 14003, 96) and anatase (James et al., 2013). Our work demonstrated that quartz is one of the least reactive mineral phases, yet there is evidence that it is most toxic to rats relative to lunar dust containing highly reactive mineral phases such as pyroxene and olivine. More work needs to be done in assessing the toxicity of individual mineral phases relative to quartz in order to determine if there are any correlations between mineral reactivity and toxicity (e.g., Caston et al., 2018). It has been shown, however, that the effects of inhaling fine particulates can have consequences that reach far beyond the respiratory system. How and why adverse bodily effects occur via inhalation of fine particulates is still unknown (Bhatnagar, 2006). There has even been evidence presented where ingestion of fine particulates, including silica and asbestos particles, can lead to the development of gastrointestinal cancers (Garcia-Perez et al., 2015; Paris et al., 2017; Santibanez et al., 2012). Inhaling fine magnetite particles has been associated with neurodegenerative diseases such as Alzheimer's disease (Maher et al., 2016). There is an abundance of similar dust particles small enough to migrate into the human nervous system, which may potentially induce similar effects presented by Maher et al. (2016). There are methods that may be worthwhile in further investigating regarding the mitigation of the toxic effects of dust inhalation. In a double-blind study conducted on nursing home residents in Mexico City, it was found that supplementation with omega-3 polyunsaturated fatty acids was able to reduce the adverse effects of exposure to particulate matter (Romieu et al., 2008). The quantitative study of planetary regolith reactivity is a field in its relative infancy (McKay et al., 2015; Meyers et al., 2012; Turci et al., 2015; Wallace et al., 2009, 2010), and while there exists a large body of work related to understanding the reactivity of toxic Earth minerals such as quartz, asbestos, and coal dust on which to build, there are aspects of reactivity that are unique to planetary surfaces which require further investigation. A further area to be explored is the effect of space weathering processes, such as surface amorphization, agglutinate formation, and nanophase iron metal production (Heiken et al., 1991; Thompson et al., 2014, 2016), on mineral reactivity (Wallace et al., 2010). Standard protocols should be developed to control for factors such as mineral grind time, incubation in spin trap solution time, time between grinding and measuring reactivity, storage conditions (i.e., temperature and humidity), and grinding methods/materials in order to be able to accurately compare mineral reactivity results between different studies. In summary, we suggest that studies designed to understand the mechanisms of mineral-induced ROS generation under conditions that accurately simulate planetary environments as well as the effects on biomolecules, cells (e.g., Caston et al., 2018), and tissues are necessary to ensure the safety and long-term health of future human explorers visiting the surfaces of planets, moons, and asteroids where fine-grained regolith materials are present.

5. Conclusions

Quantitative evaluation of OH* generation at micromolar concentrations in mineral-water slurries using EPR spectroscopy combined with spin trapping techniques has been demonstrated. Increasing the amount of time that minerals and regolith simulants are subjected to mechanical pulverization by laboratory milling results in decreased OH* generating capability, despite the fact that increased pulverization time is observed to increase total surface area in some cases. We suggest that the frictional heating that takes place as a result of longer milling times has the effect of annealing reactive surface sites and results in lower reactivity and

OH* generating capability. Increasing the amount of time that mineral and liquid solution are allowed to interact in mineral-water slurries has mixed effects that may be related to the presence or absence of iron in the mineral phase under investigation. We found that for feldspars, incubation time has little to no effect on OH* generation, suggesting either an immediate release of OH* to the mineral-water slurry or a steady state condition between OH* generation and destruction in the slurry. For nominally Fe-bearing materials (olivine, augite, and JSC-1A) and diopside, increased incubation time resulted in increased OH* concentrations, suggesting that the rate of OH* generation from these phases exceeds the rate of OH* destruction and/or that there is a cofactor involved that acts to increase the OH* generation capability of these phases. We suggest that the presence of iron in these phases may be acting as the cofactor by initiating the Fenton reaction and thereby increasing the overall OH* generation capability of Fe-bearing mineral phases. Even though more testing is required, our work points toward the hypothesis that lunar dust originating in the lunar mare exhibits higher OH* generation potential relative to dust originating in the lunar highlands. It is important to point out, however, that this in no way implies that humans working in the highlands are also not potentially susceptible to detrimental bodily effects. We show that mineral phases that generate larger amounts of OH* maintain their highly reactive state compared to those minerals which tend to generate lesser amounts of OH* (i.e., augite vs. quartz).

Acknowledgments
This study was supported by the RIS^{4}E node of the NASA Solar System Exploration Research Virtual Institute (SSERVI). We would like to thank M. Darby Dyar for her support in providing various mineral samples, as well as Jim Quinn who obtained SEM measurements for all of our mineral samples. Brookhaven National Laboratory is supported by the US Department of Energy-Office of Science. The data in this article can be accessed at Stony Brook University's Academic Commons data repository found at http://commons.library.stonybrook.edu.

References

Alshibli, K. A., & Hasan, A. (2009). Strength properties of JSC-1A lunar regolith simulant. *Journal of Geotechnical & Geoenvironmental Engineering*, *135*, 673–679. https://doi.org/10.1061/(ASCE)GT.1943-5606.0000068

Beckett, W. S. (2000). Current topics: Occupational respiratory diseases. *New England Journal of Medicine*, *342*, 406–413. https://doi.org/10.1056/NEJM200002103420607

Bhatnagar, A. (2006). Environmental cardiology- studying mechanistic links between pollution & heart disease. *Circulation Research*, *99*, 692–705. https://doi.org/10.1161/01.RES.0000243586.99701.cf

Bland, J. M., & Altman, D. G. (1986). Statistical methods for assessing agreement between two methods of clinical measurement. *Lancet*, *1*, 307–310.

Caston, R., Luc, K., Hendrix, D., Hurowitz, J. A., & Demple, B. (2018). Assessing toxicity and nuclear mitochondrial DNA damage caused by exposure of mammalian cells to lunar regolith simulants. *GeoHealth*, *2*, 139–148. https://doi.org/10.1002/2017GH000125

Cohn, C. A., Laffers, R., & Schoonen, M. A. A. (2006). Using yeast RNA as a probe for generation of OH* by Earth materials. *Environmental Science & Technology*, *40*, 2838–2843. https://doi.org/10.1021/es052301k

Cohn, C. A., Mueller, S., Wimmer, E., Leifer, N., Greenbaum, S., Strongin, D. R., & Schoonen, M. A. A. (2006). Pyrite-induced hydroxyl radical formation and its effect on nucleic acid. *Geochemical Transactions*, *7*, 3. https://doi.org/10.1186/1467-4866-7-3

Colwell, J. E., Batiste, S., Horányi, M., Robertson, S., & Sture, S. (2007). Lunar surface: Dust dynamics and regolith mechanics. *Reviews of Geophysics*, *45*, RG2006. https://doi.org/10.1029/2005RG000184

Damby, D. E., Murphy, F. A., Horwell, C. J., Raftis, J., & Donaldson, K. (2016). The in vitro respiratory toxicity of cristobalite-bearing volcanic ash. *Environmental Research*, *145*, 74–84. https://doi.org/10.1016/j.envres.2015.11.020

Dizdaroglu, M., Rao, G., Halliwell, B., & Gajewski, E. (1991). Damage to the DNA bases in mammalian chromatin by hydrogen-peroxide in the presence of ferric and cupric ions. *Archives of Biochemistry and Biophysics*, *285*, 317–324.

Dodson, R. F., Shepherd, S., Levin, J., & Hammar, S. P. (2007). Characteristics of asbestos concentration in lung as compared to asbestos concentration in various levels of lymph nodes that collect drainage from the lung. *Ultrastructural Pathology*, *31*, 95–133. https://doi.org/10.1080/01913120701423907

Doganay, S., Hayrettin, G., Yikilmaz, A., & Abdulhakim, C. (2010). Silicosis due to denim sandblasting in young people: MDCT findings. *The Eurasian Journal of Medicine*, *42*, 21–23. https://doi.org/10.5152/eajm.2010.07

Dröge, W. (2002). Free radicals in the physiological control of cell function. *Physiological Reviews*, *82*, 47–95. https://doi.org/10.1152/physrev.00018.2001

Dyar, M. D., Bryne, S. A., Bessette, E. E., Breitenfeld, L. B., Crowley, M. C., Hoff, C. M., et al. (2015). *Pure mineral separates for mixing experiments to simulate planetary surfaces*. Paper presented at the 46th Lunar & Planetary Science Conference, Houston, TX.

Eaton, G. R., Eaton, S. S., Barr, D. P., & Weber, R. T. (2010). Quantitative EPR.

Fenoglio, I., Martra, G., Prandi, L., Tomatis, M., Coluccia, S., & Fubini, B. (2001). The role of mechanochemistry in the pulmonary toxicity caused by particulate minerals. *Journal of Materials Synthesis and Processing*, *8*, 145–153. https://doi.org/1064-7562/00/0700-0145$18.00/0

Fubini, B., Fenoglio, I., Elias, Z., & Poirot, O. (2001). Variability of biological responses to silicas: Effect of origin, crystallinity, and state of surface on generation of reactive oxygen species and morphological transformation of mammalian cells. *Journal of Environmental Pathology, Toxicology and Oncology*, *20*, 95–108.

Fubini, B., & Hubbard, A. (2003). Reactive oxygen species (ROS) and reactive nitrogen species (RNS) generation by silica in inflammation and fibrosis. *Free Radical Biology and Medicine*, *34*(12), 1507–1516. https://doi.org/10.1016/s0891-5849(03)00149-7

Garcia-Perez, J., Lopez-Abente, G., Castello, A., Gonzalez-Sanchez, M., & Fernandez-Navarro, P. (2015). Cancer mortality in towns in the vicinity of installations for the production of cement, lime, plaster, and magnesium oxide. *Chemosphere*, *128*, 103–110. https://doi.org/10.1016/j.chemosphere.2015.01.020

Gilmour, P. S., Beswick, P. H., Brown, D. M., & Donaldson, K. (1995). Detection of surface free radical activity of respirable industrial fibres using supercoiled φX174 RF1 plasmid DNA. *Carcinogensis*, *16*(12), 2973–2979. https://doi.org/10.1093/carcin/16.12.2973

Haber, F., & Weiss, J. J. (1934). The catalytic decomposition of hydrogen peroxide by iron salts. *Proceedings of the Royal Society of London Series A*, *147*, 332–351.

Hardy, J. A., & Aust, A. E. (1995). Iron in asbestos chemistry and carcinogenicity. *Chemical Reviews*, *95*, 97–118. https://doi.org/10.1021/cr00033a005

Harrington, A. D., Smirnov, A., Tsirka, S. E., & Schoonen, M. A. A. (2015). Metal-sulfide mineral ores, Fenton chemistry and disease—Particle induced inflammatory stress response in lung cells. *International Journal of Hygiene and Environmental Health*, *218*, 19–27. https://doi.org/10.1016/j.ijheh.2014.07.002

Harrington, A. D., Tsirka, S. E., & Schoonen, M. A. A. (2012). Quantification of particle-induced inflammatory stress response: A novel approach for toxicity testing of earth materials. *Geochemical Transactions*, *13*, 10. https://doi.org/10.1186/1467-4866-13-4

Harrington, A. D., Tsirka, S. E., & Schoonen, M. A. A. (2013). Inflammatory stress response in A549 cells as a result of exposure to coal: Evidence for the role of pyrite in coal workers' pneumoconiosis pathogenesis. *Chemosphere*, *93*, 1216–1221. https://doi.org/10.1016/j.chemosphere.2013.06.082

Hasegawa, M., Ogata, T., & Sato, M. (1995). Mechano-radicals produced from ground quartz and quartz glass. *Powder Technology*, *85*, 269–274. https://doi.org/10.1016/0032-5910(96)80150-1

Heiken, G., Vaniman, D. T., & French, B. M. (1991). The lunar sourcebook, a user's guide to the Moon.

Hickson, J. C., & Juras, S. J. (1986). Sample contamination by grinding. *Canadian Mineralogist*, *24*, 585–589.

Hill, E., Mellin, M. J., Deane, B., Liu, Y., & Taylor, L. A. (2007). Apollo sample 70051 and high- and low-Ti lunar soil simulants MLS-1A and JSC-1A: Implications for future lunar exploration. *Journal of Geophysical Research*, *112*, E02006. https://doi.org/10.1029/2006JE002767

Horwell, C. J., Baxter, P. J., Hillman, S. E., Calkins, J. A., Damby, D. E., Delmelle, P., et al. (2013). Physicochemical and toxicological profiling of ash from the 2010 and 2011 eruptions of Eyjafjallajokull and Grimsvotn volcanoes, Iceland using a rapid respiratory hazard assessment protocol. *Environmental Research*, *127*, 63–73. https://doi.org/10.1016/j.envres.2013.08.011

Horwell, C. J., Fenoglio, I., Ragnarsdottir, K. V., Sparks, R. S. J., & Fubini, B. (2003). Surface reactivity of volcanic ash from the eruption of Soufriere Hills volcano, Montserrat, West Indies with implications for health hazards. *Environmental Research*, *93*, 202–215. https://doi.org/10.1016/S0013-9351(03)00044-6

Horwell, C. J., Fenogolio, I., & Fubini, B. (2007). Iron-induced OH* generation from basaltic volcanic ash. *Earth and Planetary Science Letters*, *261*(3–4), 662–669. https://doi.org/10.1016/j.epsl.2007.07.032

Hurowitz, J. A., Tosca, N. J., McLennan, S. M., & Schoonen, M. A. A. (2007). Production of hydrogen peroxide in Martian and lunar soils. *Earth and Planetary Science Letters*, *255*, 41–52. https://doi.org/10.1016/j.epsl.2006.12.004

James, J. T., Lam, C.-W., Santana, P., & Scully, R. R. (2013). Estimate of safe human exposure levels for lunar dust based on comparative benchmark does modeling. *Inhalation Toxicology*, *25*, 243–256. https://doi.org/10.3109/08958378.2013.777821

Kaur, J., Rickman, D., & Schoonen, M. A. A. (2016). Reactive oxygen species (ROS) generation by lunar simulants. *Acta Astronautica*, *122*, 196–208. https://doi.org/10.1016/j.actaastro.2016.02.002

Khan-Mayberry, N. (2008). The lunar environment: Determining the health effects of exposure to moon dusts. *Acta Astronautica*, *63*, 1006–1014. https://doi.org/10.1016/j.actaastro.2008.03.015

King, E. J., Rogers, N., Gilchrist, M., Goldschmidt, V. M., & Nagelschmidt, G. (1945). The effect of olivine on the lungs of rats. *Journal of Pathology and Bacteriology*, *57*, 488–491.

Latch, J. M., Hamilton, R. F., Holian, A., James, J. T., & Chiu-Wing, L. (2008). Toxicity of lunar and Martian dust simulants to alveolar macrophages isolated from human volunteers. *Inhalation Toxicology*, *20*, 157–165. https://doi.org/10.1080/08958370701821219

Linnarsson, D., van Westrenen, W., Carpenter, J., Fubini, B., Gerde, P., Karlsson, L. L., et al. (2012). Toxicity of lunar dust. *Planetary and Space Science*, *74*, 57–71. https://doi.org/10.1016/j.pss.2012.05.023

Loftus, D. J., Rask, J. C., McCrossin, C. G., & Tranfield, E. M. (2010). The chemical reactivity of lunar dust: From toxicity to astrobiology. *Earth, Moon, and Planets*, *107*, 95–105. https://doi.org/10.1111/j.1468-4004.2010.51411.x

Maher, B. A., Ahmed, I. A. M., Karloukovski, V., MacLaren, D. A., Foulds, P. G., Allsop, D., et al. (2016). Magnetite pollution nanoparticles in the human brain. *Proceedings of the National Academy of Sciences of the United States of America*, *113*, 10,797–10,801. https://doi.org/10.1073/pnas.1605941113

Makino, K., Hagiwara, T., Hagi, A., & Murakami, A. (1990). Cautionary note for DMPO spin trapping in the presence of iron ion. *Biochemedical Biophysical Research Communications*, *173*(2), 1073–1080.

McKay, D. S., Cooper, B. L., Taylor, L. A., James, J. T., Thomas-Keprta, K. L., Pieters, C. M., et al. (2015). Physicochemical properties of respirable-size lunar dust. *Acta Astronautica*, *107*, 163–176. https://doi.org/10.1016/j.actaastro.2014.10.032

Meyers, V. E., Garcia, H. D., Monds, K., Cooper, B. L., & James, J. T. (2012). Ocular toxicity of authentic lunar dust. *BMC Ophthalmology*, *12*. https://doi.org/10.1186/1471-2415-12-26

Nakamura, K., Kanno, T., Ikai, H., Sato, E., Mokudai, T., Niwano, Y., Ozawa, T., et al. (2010). Reevaluation of quantitative ESR spin trapping analysis of OH* by applying sonolysis of water as a model system. *Bulletin of the Chemical Society of Japan*, *83*, 1037–1046. https://doi.org/10.3164/jcbn.10-125

Orberdörster, G., Orberdörster, E., & Orberdörster, J. (2005). Nanotoxicology: An emerging discipline evolving from studies of ultrafine particles. *Environmental Health Perspectives*, *113*, 823–839. https://doi.org/10.1289/ehp.7339

Paris, C., Thaon, I., Herin, F., Clin, B., Lacourt, A., Luc, A., et al. (2017). Occupational asbestos exposure and incidence of colon and rectal cancers in French men: The asbestos-related diseases cohort (ARDCo-Nut). *Environmental Health Perspectives*, *125*, 409–415. https://doi.org/10.1289/EHP153

Pezerat, H. (1991). In R. C. Brown, J. A. Hoskins, & N. F. Johnson (Eds.), *Mechanisms in Fibre Carcinogenesis* (pp. 387–395). New York: Plenum Press.

Pryor, W. A. (1988). Why is the OH* the only radical that commonly adds to DNA—Hypothesis—It has a rare combination of high electrophilicity, high thermochemical reactivity, and a mode of production that can occur near DNA. *Free Radical Biology and Medicine*, *4*, 219–223.

Rice-Evans, C. A., Diplock, A. T., & Symons, M. C. R. (1991). Techniques in free radical research, laboratory techniques in biochemistry and molecular biology. *Federation of European Biochemical Societies*, *22*, 291.

Rimal, B., Greenberg, A. K., & Rom, W. N. (2005). Basic pathogenetic mechanisms in silicosis: Current understanding. *Current Opinion in Pulmonary Medicine*, *11*, 169–173. https://doi.org/10.1097/01.mcp.0000152998.11335.24

Romieu, I., Garcia-Esteban, R., Sunyer, J., Rios, C., Akaraz-Zubeldia, M., Velasco, S. R., & Holguin, F. (2008). The effect of supplementation with omega-3 polyunsaturated fatty acids on markers of oxidative stress in elderly exposed to PM (2.5). *Environmental Health Perspectives*, *116*, 1237–1242. https://doi.org/10.1289/ehp.10578

Santana, P. A., James, J. T., & Lam, C.-W. (2010). Modeling respiratory toxicity of authentic lunar dust. NASA Report JSC-CN-22387.

Santibanez, M., Alguacil, J., de la Hera, M. G., Navarrete-Munoz, E. M., Llorca, J., Aragones, N., et al. (2012). Occupational exposures and risk of stomach cancer by histological type. *Occupational and Environmental Medicine*, *69*, 268–275. https://doi.org/10.1136/oemed-2011-100071

Scheuring, R. A., Jones, J. A., Novak, J. D., Polk, J. D., Gillis, D. B., Schmid, J., et al. (2008). The Apollo medical operations project: Recommendations to improve crew health and performance for future exploration missions and lunar surface operations. *Acta Astronautica*, *63*, 980–987. https://doi.org/10.1016/j.actaastro.2007.12.065

Schoonen, M. A. A., Cohn, C. A., Roemer, E., Laffers, R., Simon, S. R., & O'Riordan, T. (2006). Mineral-induced formation of reactive oxygen species. *Reviews in Mineralogy and Geochemistry*, *64*, 179–221. https://doi.org/10.2138/rmg.2006.64.7

Schoonen, M. A. A., Harrington, A. D., Laffers, R., & Strongin, D. R. (2010). Role of hydrogen peroxide and OH* in pyrite oxidation by molecular oxygen. *Geochimica et Cosmochimica Acta*, *74*, 4971–4987. https://doi.org/10.1016/j.gca.2010.05.028

Selby, J. V., & Friedman, G. D. (1988). Epidemiologic evidence of an association between body and iron stores and risk of cancer. *International Journal of Cancer*, *41*, 677–682.

Stevens, R. G., Beasley, R. P., & Blumberg, B. S. (1986). Iron-binding proteins and risk of cancer in Taiwan. *Journal of the National Cancer Institute*, *76*, 605–610. https://doi.org/10.1093/jnci/76.4.605

Taraborrelli, D., Lawrence, M. G., Crowley, J. N., Dillon, T. J., Gromov, S., Grosse, C. B. M., et al. (2012). OH* buffered by isoprene oxidation over tropical forests. *Nature Geoscience*, *5*, 190–193. https://doi.org/10.1038/ngeo1405

Thompson, M. S., Chistoffersen, R., Zega, T. J., & Keller, L. P. (2014). Microchemical and structural evidence for space weathering in soils from asteroid Itokawa. *Earth, Planets and Space*, *66*. https://doi.org/10.1186/1880-5981-66-89

Thompson, M. S., Zega, T. J., & Howe, J. Y. (2016). *Simulation of micrometeorite impacts through in-situ dynamic heating of lunar soil*. Paper presented at the 47th Lunar & Planetary Science Conference, Houston, TX.

Turci, F., Corazzari, I., Alberto, G., Martra, G., & Fubini, B. (2015). Free-radical chemistry as a means to evaluate lunar dust health hazard in view of future missions to the Moon. *Astrobiology*, *15*, 371–380. https://doi.org/10.1089/ast.2014.1216

Vallyathan, V., Leonard, S., Kuppusamy, P., Pack, D., Chzhan, M., Sanders, S. P., & Zweir, J. L. (1997). Oxidative stress in silicosis: Evidence for the enhanced clearance of free radicals from whole lungs. *Molecular and Cellular Biochemistry*, *168*, 125–132. https://doi.org/10.1023/A:1006850920080

Von Sonntag, C., Glass, W., & Varma, M. (1991). In W. A. Glass & M. N. Varma (Eds.), *Physical and chemical mechanisms in molecular radiation biology* (Vol. 58, pp. 231–287). New York: Plenum Press.

Wagner, S. (2004). *An assessment of dust effects on planetary surface systems to support exploration requirements* (Report No. CTSD-AIM-0029). Houston, TX: NASA Johnson Space Center.

Wallace, W. T., Phillips, C. J., Jeevarajan, A. S., Chen, B., & Taylor, L. A. (2010). Nanophase iron-enhanced chemical reactivity of ground lunar soil. *Earth and Planetary Science Letters*, *295*, 571–577. https://doi.org/10.1016/j.epsl.2010.04.042

Wallace, W. T., Taylor, L. A., Liu, Y., Cooper, B. L., McKay, D. S., Chen, B., & Jeevarajan, A. S. (2009). Lunar dust and lunar simulant activation and monitoring. *Meteoritics & Planetary Science*, *44*, 961–970. https://doi.org/10.1111/j.1945-5100.2009.tb00781.x

Zeng, X., He, C., Oravec, H., Wilkinson, A., Agui, J., & Asnani, V. (2010). Geotechnical properties of JSC-1A lunar soil simulant. *Journal of Aerospace Engineering*, *23*(2), 111–116. https://doi.org/10.1061/(ASCE)AS.1943-5525.0000014

Zhou, X., Beine, H. J., Honrath, R. E., Fuentes, J. D., Simpson, W., Shepson, P. B., & Bottenheim, J. W. (2001). Snowpack photochemical production of HONO: A major source of OH in the Arctic boundary layer in springtime. *Geophysical Research Letters*, *28*, 4087–4090. https://doi.org/10.1029/2001GL013531